Title pages

Title

Fully Automatic Quantification for Hand Synovitis in Rheumatoid Arthritis Using Pixel-Classification-based Segmentation Network in DCE-MRI

Wanxuan Fang[1], Yijun Mao[2], Haolin Wang[3], Hiroyuki Sugimori[4], Shinji Kiuch[5], Kenneth Sutherland[6] and Tamotsu Kamishima[7]

1 Graduate School of Health Sciences, Hokkaido University

North-12 West-5, Kita-ku, Sapporo, 060-0812, Japan

E-mail: fangwanxuan2020@163.com

2 Graduate School of Health Sciences, Hokkaido University

North-12 West-5, Kita-ku, Sapporo, 060-0812, Japan

E-mail: Mao_YiJun0731@hotmail.com

3 Graduate School of Health Sciences, Hokkaido University

North-12 West-5, Kita-ku, Sapporo, 060-0812, Japan

E-mail: haolin.wang.k3@elms.hokudai.ac.jp

4 Faculty of Health Sciences, Hokkaido University

North-12 West-5, Kita-ku, Sapporo, 060-0812, Japan

E-mail: sugimori@hs.hokudai.ac.jp

5 AIC Yaesu Clinic

C-road Bldg., 2-1-18, Nihonbashi, Chuo-ku, Tokyo, Japan.

E-mail: kiuchi@m-satellite.jp

6 Global Center for Biomedical Science and Engineering, Hokkaido University

North-15 West-7, Kita-ku, Sapporo 060-8638, Japan

E-mail: kensuth@med.hokudai.ac.jp

7 Faculty of Health Sciences, Hokkaido University

North-12 West-5, Kita-ku, Sapporo, 060-0812, Japan

E-mail: ktamotamo2@gmail.com

Address correspondence to:

Tamotsu Kamishima, MD, PhD,

Faculty of Health Sciences, Hokkaido University

North-12, West-5, Kita-ku, Sapporo 060-0812, Japan

Phone; 81-11-706-2824

E-mail; ktamotamo2@gmail.com

http://www.hs.hokudai.ac.jp/kamishima/index.html

Abstract

Purpose: A classification-based segmentation method is proposed to quantify synovium in rheumatoid arthritis (RA) patients using a deep learning (DL) method based on time-intensity curve (TIC) analysis in dynamic contrast-enhanced magnetic resonance imaging (DCE-MRI).

Materials and methods: This retrospective study analyzed a hand MR dataset of 28 RA patients (six males, mean age 53.7 years). A researcher, under expert guidance, used in-house software to delineate regions of interest (ROIs) for hand muscles, bones, and synovitis, generating a dataset with 27255 pixels with corresponding TICs (muscle: 11413, bone: 8502, synovitis: 7340). One experienced musculoskeletal radiologist performed ground truth segmentation of enhanced pannus in the joint bounding box on the 10^{th} DCE phase, or around 5 minutes after contrast injection. Data preprocessing included median filtering for noise reduction, phase-only correlation algorithm for motion correction, and contrast-limited adaptive histogram equalization for improved image contrast and noise suppression. TIC intensity values were normalized using zero-mean normalization. A DL model with dilated causal convolution and SELU activation function was developed for enhanced pannus segmentation, tested using leave-one-out cross-validation.

Results: 407 joint bounding boxes were manually segmented, with 129 synovitis masks. On the pixel-based level, the DL model achieved sensitivity of 85%, specificity of 98%, accuracy of 99% and precision of 84% for enhanced pannus segmentation, with a mean Dice score of 0.73. The false positive rate for predicting cases without synovitis was 0.8%. DL-measured enhanced pannus volume strongly correlated with ground truth at both pixel-based ($r = 0.87$, $p < 0.001$) and patient-based levels ($r = 0.84$, $p < 0.001$). Bland-Altman analysis showed the mean difference for hand joints at the pixel-based and patient-based levels were -9.46mm^3 and -50.87mm^3, respectively.

Conclusion: Our DL-based DCE-MRI TIC shape analysis has the potential for automatic segmentation and quantification of enhanced synovium in the hands of RA patients.

Keywords: Rheumatoid Arthritis, Dynamic Contrast-Enhanced Magnetic Resonance Imaging, Synovitis, Deep Learning, Quantitative Analysis

Secondly Abstract

We proposed a classification-based segmentation method to quantify synovium in rheumatoid arthritis (RA) patients using a deep learning method based on time-intensity curve analysis in dynamic contrast-enhanced magnetic resonance imaging. It has the potential for quick and accurate assessment of enhanced synovium in the hands of RA patients.

Text

Introduction

Rheumatoid arthritis (RA) is an incurable chronic autoimmune disease characterized by inflammation of the synovial joints, leading to severe functional impairment and disability [1, 2]. Imaging has highlighted and substantiated that not only bone marrow edema is a reliable predictor of erosive progression, but also synovitis correlates with the development of radiographic bone erosions [3, 4]. Synovitis is considered the best predictor marker of joint damage [5]. Furthermore, synovial volume correlates with joint swelling and tenderness and the rate of erosion progression associated with baseline synovial volume [6]. As a consequence, accurate quantification and early detection of synovitis play an important role in the clinical evaluation and treatment of RA.

Magnetic resonance imaging (MRI) allows soft-tissue assessment of joint structures, including the synovium, cartilage, and bone marrow, among other articular structures [6]. Dynamic contrast-enhanced MRI (DCE-MRI) is based on the perfusion dynamics of synovial enhancement curves after contrast injection and has been found to correlate with synovial histopathological inflammation [7]. It has also been used to assess inflamed synovial membranes and allow quantification of the synovium's volume [8, 9]. Thus, DCE-MRI may enable an accurate assessment of the disease activity based on a selected region of interest [7].

In recent years, many researchers focused on using time-intensity curve (TIC) shape analysis in DCE-MRI to quantify synovitis of RA [10-13]. Pixel-by-pixel TIC shape analysis is a new dynamic contrast-enhanced MRI technique to help visualize differently shaped TICs [11]. In a previous study, pixels with TIC shape type 4, characterized as early enhancement followed by washout phase, were regarded as synovitis pixels [10]. TIC shape analysis may be an alternative to the gold standard of manual

contouring for pannus quantification was demonstrated using pixel-by-pixel TIC shape analysis [11]. Unfortunately, this study [11] has difficulty discriminating artery pixels and may quantify synovitis of RA inaccurately. The arterial mask subtraction method with mutual information has been proposed to improve the accuracy of pixel-by-pixel TIC shape analysis in dynamic MRI [10]. Although the result was promising in this study, this method has not been put into practice because it takes a long time to analyze.

Automated synovitis segmentation and quantification methods have important potential advantages, including speed, accuracy, and consistency. Deep learning (DL) has been used for various musculoskeletal imaging applications, including tissue segmentation, image reconstruction, and disease detection [14, 15]. One-dimensional convolutional neural network (1D-CNN) models work well for time-series signals and is now being used for the classification of cardiotocographic signals [16], detection of epileptic seizure [17], and detection of atrial fibrillation [18] amongst others. We therefore hypothesized that the segmentation and quantification of RA hand synovitis based on TIC shape can be performed using a 1D-CNN.

The purpose of this study was to automatically segment and quantify enhanced synovial membranes in patients with inflammatory arthritis on DCE-MRI based on TIC curves by 1D-CNN using a radiologist's assessment as the gold standard.

Materials and Methods

Subjects and MRI Dataset

The requirement of written informed consent was waived by the Institutional Ethics Committee owing to the retrospective study design. In this retrospective study, both hands were analyzed using DCE-

MRIs, involving 28 rheumatoid patients (twenty-two females and six males) aged 17 to 82 years, with a mean age of 53.7 years. All patients met the criteria set forth by the American College of Rheumatology (ACR) and the European League Against Rheumatism for the year 2010 classification for RA at the time of their inclusion [19]. The inclusion criteria for this arthritis cohort necessitated the presence of active arthritis in the wrist or finger joints based on clinical assessments, although the specific extent of the disease was not specified.

The subjects were positioned for imaging in a 3.0-T MR scanner (Ingenia; Philips Medical Systems, Best, Netherlands) using the mDixon water algorithm. DCE-MRI coronal data were collected using TR/TE/TE = 5.4 /1.35 / 2.4 msec, acquisition matrix = 512 × 512, field of view (FOV) = 240 × 240 to 307.2 × 307.2 mm, bandwidth = 1184 to 1497 Hz per pixel, flip angle = 10º at 2 mm section thickness, and number of slices 18 or 27, phase 55 to 68, coronal orientation). At the initiation of the first phase acquisition, the contrast agent (0.2 mL per kilogram of body weight of gadopentetate dimeglumine; Magnescope; Guerbet, Paris, France) was administrated via an automatic MR injection device (SonicShot GX; Nemoto Kyorindo). The imaging process encompassed the bilateral hands, with subjects positioned in a prone posture while extending both arms over their heads.

Overview of analysis

A classification-based segmentation method is proposed in this study to quantify the enhanced synovium in RA patients using a DL method based on TIC analysis in DCE-MRI. One researcher delineated regions of interest (ROIs) for hand muscles, bones, and synovitis with in-house software under expert guidance, acquiring a dataset of TICs representing signal intensity variation over time for each voxel. Ground truth segmentation of enhanced pannus in the joint bounding box was performed by a

musculoskeletal (MSK) radiologist. Our synovitis segmentation network underwent training, testing, and evaluation using leave-one-out cross-validation on 28 subjects with randomized dataset shuffling. The specific content regarding the research methodology is divided into the following subsections: acquisition of TICs, dataset labeling, data preprocessing, synovitis segmentation method, training and testing of the synovitis segmentation software, and statistical analysis.

Acquisition of TICs

One researcher set ROIs in the muscle, bone, and synovitis on DCE-MR images and processed them using an internally developed software program running on MATLAB (Mathworks, Natick, Mass, USA). This program analyzes the time-dependent signal intensity changes of each voxel within the ROIs to create TICs and obtain detailed intensity information for each voxel (Fig.1). For muscles and bones, the ROI placement involved avoiding blood vessels, bony cortex, and tendons, choosing slices where hand muscles and bones were distinctly visible, and delineating ROIs in central areas to ensure their area was smaller than that of muscles and bones. The selection of the synovitis ROI involved several steps: avoiding vascular regions, identifying the most intensely enhanced portion as the synovitis ROI, and adapting the ROI size based on the lesion's size, ensuring that the ROI's area remained smaller than that of the synovitis. When obtaining the TIC, the ROI size should not be smaller than 4 pixels. These were done under the supervision of an MSK radiologist (T.K.) with over 30 years of experience.

Dataset Labeling

The enhanced synovitis masks of 28 subjects were manually labeled by a MSK radiologist using the software ImageJ (version 1.53h, National Institutes of Health, Bethesda, Bethesda, MA, USA) on

coronal MRI slices. According to the Rheumatoid Arthritis Magnetic Resonance Imaging Scoring System (RAMRIS) criteria [20], 14 primary bounding boxes were defined for each hand, encompassing the metacarpophalangeal (MCP) joints (excluding the 1st MCP joint), distal radioulnar joint (DRUJ), radiocarpal joint (RCJ), as well as intercarpal and carpometacarpal joints (ICJ). Joints with notably intensified synovitis were also included. The detailed labeling process was as follows:

1. A bounding box was established around the chosen joints to encompass all the enhanced synovitis on that particular MRI slice.
2. The enhanced synovitis masks enclosed within the bounding box were meticulously outlined manually
3. The bounding boxes for finger joints without synovitis were placed centrally on the joints, avoiding the inclusion of adjacent joints.

For synovitis labeling, DCE-MRI images captured on the 10th phase or around 5 minutes after contrast injection were chosen. The manually segmented synovitis masks served as the gold standard [11], and the synovitis area was computed automatically.

Data Preprocessing

In the field of medical image processing, image preprocessing is performed to enhance the accuracy and reliability of subsequent analyses, as shown in Fig. 2. Firstly, a median filter with a kernel size of 3x3 was first applied to DCE-MRI images to mitigate the adverse effects of noise. Secondly, to account for motion misalignment in the images, the phase-only correlation algorithm [21] was employed for image registration. The offset between phases with the most obvious features of synovitis was computed, and dynamic MRI image registration was performed using the mean offset. Thirdly, contrast limited

adaptive histogram equalization (CLAHE) [22] was utilized to enhance overall image contrast while suppressing noise. Subsequently, to address variations in overall MRI image brightness across cases, Otsu thresholding was performed to segment the background in the selected DCE-MRI slice. We then computed the mean of pixels within the 50% confidence interval for the foreground, achieving intensity balance. The ratio of the intensity of training data sampled from this slice to the mean was computed to obtain relative intensity values. To ensure uniform analysis across cases with varying phase lengths, linear interpolation was utilized to standardize all-time series to a length of 27 phases, ensuring data consistency and facilitating analysis across all samples. Finally, relative intensity values were extracted using in-house software and normalized for training purposes through zero-mean normalization (ZMN).

Synovitis Segmentation Method

A novel 1D CNN is proposed for automatic classification-based tissue segmentation using DCE-MRI temporal intensity signal data as input. In the proposed network, dilated causal convolution [23] and the scaled exponential linear unit (SELU) activation function are utilized to classify three distinct categories: muscle, bone, and synovitis. Dilated causal convolution is a widely utilized convolutional operation for feature extraction in sequence data, with several notable advantages, including the expansion of the receptive field, parameter count reduction, and support for parallel processing. Moreover, it excels in the swift acquisition of causal relationships within extensive time series data. The SELU activation function represents a self-normalizing function with distinctive characteristics that mitigate the problem of neurons halting their learning process. In contrast to traditional activation functions, SELU proves more effective in addressing issues related to gradient vanishing and explosion.

The network architecture, shown in Fig. 3, comprises a feature extraction part, consisting of four identical layers stacked. Each layer includes dilated causal convo lution, batch normalization, and the SELU activation function. The parameters for dilated causal convolution are set as dilated factors 1, 2, 2, output channels 128, 256, 128, and kernel size 8, 5, 3 when the layer depth is 1, 2, 3, as depicted in Fig. 3. Batch normalization is incorporated to ensure uniform distribution of inputs for each layer, while the SELU activation function is employed for non-linear transformation of the input, generating the output at each layer. Global average pooling and softmax are added following the stack layer to extract feature vectors and calculate the probability for each class to achieve multi-classification. The detailed network structure is illustrated in Table 1.

The proposed network was implemented using the Python language and the PyTorch package on a workstation equipped with a CPU. The loss function consisted of sigmoid and BCELoss.

Training and Testing of the Synovitis Segmentation Network

Due to the relatively small size of the dataset, to enhance the reliability of the network, leave-one-out cross-validation was performed on 28 subjects by randomly shuffling the dataset. In each fold of the cross-validation process, 27 sets of patient data were shuffled during training and validation, while the data for the remaining patient was used for testing. This process was repeated 28 times in an alternating manner.

The training and testing framework of the proposed method is illustrated in Fig. 4. In the training phase, the reference standard for training the classification network was labeled for the corresponding TICs in different regions by manually delineating various tissue regions within each set of images, provided by an MSK radiologist. The network acquires the ability to classify pixels by utilizing time-

intensity data and associated labels. The network was trained using the Adam optimizer with a learning rate of 0.00001, which was halved when there was no decline in the loss for two consecutive epochs. The training was comprised of 20 epochs with a batch size of 128.

In the testing phase, the reference standard for testing the network was masks of different tissue regions provided by an MSK radiologist. The network receives a series of dynamic MRI image sequences as input and conducts pixel-level classification predictions within the specified region to produce segmentation results.

Statistical Analysis

Pixels with TIC shape 4 were considered synovitis pixels, characterized by early enhancement followed by a washout phase [24]. The number of synovitis pixels for each bounding box was automatically obtained separately through software and manual delineation. Based on the pixel count, the volume of synovitis could be calculated using the following formula:

$$\text{Synovial membrane volume } (mm^3)$$

$$= \text{number of synovitis pixels } \times \text{ pixel size } (mm^2) \times \text{ slice thickness } (mm)$$

Pearson's correlation analysis was conducted to evaluate the correlation between the volume of synovitis obtained from software and manual delineation at pixel- and patient-based levels. The consistency of synovitis volume at both pixel-based and patient-based levels was assessed using Bland-Altman plots. Pixel-based statistical analysis was conducted to assess the volume of synovitis within each bounding box containing positive synovitis, while patient-based statistical analysis was performed on the cumulative volume of synovitis across all bounding boxes containing positive synovitis for each patient. Statistical analysis was performed using the Statistical Packages for Social Sciences (SPSS,

version 26; SPSS, Chicago, Illinois, USA) and GraphPad Prism (version 9.0 GraphPad Software Inc., USA), with the significance level set at $p < 0.05$. Pearson's correlation coefficients were set as follows: $r = 0 - 0.3$, weak correlation; $r = 0.3 - 0.7$, moderate correlation; $r > 0.7$, strong correlation [25].

The segmentation performance of the software was evaluated using the Dice similarity coefficient (DSC), sensitivity, specificity, accuracy, precision, and false positive rate (FPR) on pixel-based level. These metrics were based on whether the computer software correctly or incorrectly identified a pixel compared to the manual segmentation (ground truth). The Dice score determined the spatial overlap between manual segmentation and network segmentation.

Results

For the acquisition of TIC curves, ROIs in the muscle, bone, and synovitis regions on DCE-MRI images were placed (muscle; 34, bone; 44, and synovitis; 106); The dataset included 27255 pixels with corresponding TICs (muscle: 11413, bone: 8502, synovitis: 7340).

For dataset labeling, manual segmentation was performed on 407 joint bounding boxes. Within 129 joint bounding boxes with positive synovitis (including 74 finger joints and 55 wrist joints), manual segmentation was carried out for synovitis masking. This included joints with significantly enhanced synovitis. Additionally, 278 joint bounding boxes indicated negative synovitis. Illustrative examples of pixel-wise segmentation of synovitis cases in finger and wrist joints using the software are presented in Fig. 5. For the patient-level analysis, 24 patients exhibited evident synovitis, prompting the placement of joint bounding boxes and manual delineation of positive synovitis. The remaining 4 patients showed no apparent synovitis in the hand joints; hence, joint bounding boxes were placed without manual delineation.

On the pixel-based level, the performance of the deep learning model for synovitis segmentation was evaluated through leave-one-out cross-validation, with an average sensitivity of 85% ± 0.21, specificity of 98% ± 0.04, accuracy of 99% ± 0.01, and precision of 84% ± 0.19,. The FPR for predicting cases without synovitis symptoms was as low as 0.8% ± 0.02. The average cross-validated Dice score for synovitis segmentation was 0.73. In terms of specific regions, the wrist area exhibited a higher Dice score (0.78), whereas the finger region typically showed slightly lower values (Dice score of 0.7).

The scatter plot in Fig. 6 exhibited a strong correlation between the volumes of enhanced synovitis measured by the deep learning model and those manually delineated at both pixel-based (Fig.6A: $r = 0.87$, $p < 0.001$) and patient-based levels (Fig.6B: $r = 0.84$, $p < 0.001$). Fig. 7 presents a Bland-Altman analysis chart for software and manual synovitis segmentation at pixel-based (Fig.7A) and patient-based levels (Fig.7B) to demonstrate the consistency between deep learning and manual segmentation. Compared to manual delineation, the network measurements systematically exceeded by 9.46% at the pixel-based level. Compared to manual delineation, the network measurements systematically exceeded by 50.87% at the patient-based level. Fig.8 displays examples of the software results corresponding to outliers with absolute differences greater than 100 ml in the Bland-Altman plot at the pixel-based level.

Time-saving analysis in quantitative synovitis measurements indicated that the well-trained network could predict the measurement of a bounding box in just 1 second.

Discussion

The evaluation of RA patients relies on accurate and reproducible quantitative measurements of synovitis to assess disease activity. In this study, we employed a TIC curve analysis-based AI approach using DCE-MRI to automatically segment and quantify synovium enhancement in the hands of RA

patients. On both pixel-based and patient-based levels, the synovitis segmentation algorithm demonstrated a strong correlation with manual delineation. And on pixel-based level, the software segmentation exhibited high accuracy, precision, sensitivity, and specificity in identifying enhanced synovitis, with an exceptionally low FPR in predicting bounding boxes without synovitis. In addition, the time required for the software to automatically segment a bounding box within synovitis was only 1 second compared to several minutes for manual contouring.

A decade ago, Kubassova et al. [26] developed Dynamika-RA which can effectively reduce motion artifacts and shorten the evaluation time of MRI synovial inflammation in RA patients, offering an automated approach to data analysis. However, this method only analyzes the relevant parameters of the TIC such as maximum enhancement, initial rate of enhancement, and time of onset of enhancement and does not provide a volumetric assessment of synovitis. Czaplicka et al. [27] introduced an automated approach for quantifying synovial membrane volume in wrist joints through DCE-MRI. Their study showed comparable correlations between automatically and manually quantified synovitis volumes and RAMRIS scores. However, it is important to note that this method was limited to the automation of synovitis quantification in the wrist joint and is time-consuming, requiring a total of 10 minutes for the quantification of synovitis in the wrist joint.

Our software holds many potential clinical values. Traditionally, methods for quantifying synovitis in MRI included semi-quantitative approaches like RAMRIS [20] and quantitative methods involving manual delineation [6]. Unfortunately, these methods are subjective and susceptible to operator skill level and training, resulting in lower accuracy and reproducibility than deep learning models. The delineation of synovitis contours, often irregular lesions, typically demands a considerable amount of time, leading to operator fatigue, especially when high precision is required at contour boundaries, where human errors

may naturally occur. In contrast, in this study, our deep learning method can achieve accuracy levels similar to or exceeding those of previous studies and perform automatic detection and segmentation of synovitis lesions in hand DCE-MRI images of RA patients, thereby indicating the location of synovitis. Additionally, our software is fully automated, making it highly efficient for detecting synovitis within the bounding box of the hand (1 second), which enables it to serve as a rapid screening method for synovitis. This significantly reduces the workload of radiologists. Our software is also not influenced by errors related to inexperience, distraction, and fatigue associated with human interpretation of medical images.

Although the model showed robust performance, the results of the Bland-Altman plot reveal that the volumes of synovitis measured by the software are mostly greater than those manually delineated. This discrepancy can be attributed to the similarity in the TIC shapes between synovitis, tenosynovitis, and blood vessels in DCE-MRI. The software's quantitative measurement sometimes misidentifies vessels and tenosynovitis within the measurement area as synovitis, leading to an overestimation. The lower Dice score in software segmentation of enhanced pannus is also attributable to this issue. Furthermore, the low segmentation accuracy also stems from the inaccuracy in manual delineation. The irregular shape and relatively small size of enhanced synovitis in the hand make manual delineation challenging to achieve high precision. Discerning certain synovitis lesions from adjacent vessels in coronal images poses a formidable challenge to the naked eye. This observation underscores the capability of the software to detect synovitis that is challenging for the naked eye to distinguish.

This study has some limitations. The current software is unable to identify and differentiate bone erosions and bone marrow edema. These limitations can be addressed through more meticulous manual delineation and optimization of model parameters. Despite these edge cases, the software remains more

objective and significantly reduces the workload of radiologists. The other limitation is that deep learning research typically requires large amounts of data to achieve good results. The number of subjects in the synovitis dataset was relatively small in comparison to what is usually required for deep learning. Despite the small number of patients, the quantity of training data was sufficient (muscle: 11413, bone: 8502, synovitis: 7340).

The ultimate constraint lies in the absence of an external validation dataset. In the case of patients diagnosed with RA, DCE-MRI is not a customary standard procedure. Additionally, our investigation is an introductory AI study focused on assessing the viability of automatically delineating synovitis through TIC classification. External validation is planned for future research endeavors.

To the best of our knowledge, this study is the first to perform fully automated segmentation of synovitis in the hands of RA patients based on TIC curves on DCE-MRI. The proposed network demonstrates fully automated synovitis segmentation's feasibility and reasonable accuracy. This method is more objective and might significantly reduce the workload of radiologists, thus optimizing the management of patients with RA.

Acknowledgements

We would like to express our sincere gratitude to Yujie An, MS for her invaluable assistance in the processing and analysis of experimental data.

Declarations

Funding

This work was supported by JST SPRING, Grant Number JPMJSP2119。

Competing Interest

The authors declare that they have no conflict of interest.

Ethics approval

The study was approved by the institutional ethics committee of the Faculty of Health Sciences, Hokkaido University, and the study was performed in accordance with the ethical standards as laid down in the 1964 Declaration of Helsinki and its later amendments.

Informed Consent

Informed consent was waived.

Data Availability

Scientific data pertaining to this study is unavailable due to the absence of consent from the patients involved, in adherence to ethical guidelines and privacy considerations.

References:

1. Dakkak YJ, Jansen FP, DeRuiter MC, Reijnierse M, van der Helm-van Mil AHM. Rheumatoid Arthritis and Tenosynovitis at the Metatarsophalangeal Joints: An Anatomic and MRI Study of the Forefoot Tendon Sheaths. Radiology. 2020;295(1):146-54.
2. Micu MC, Fodor D. Concepts in monitoring the treatment in rheumatoid arthritis- the role of musculoskeletal ultrasound. Part I: synovitis. Med Ultrason. 2015;17(3):367-76.
3. Schett G, Gravallese E. Bone erosion in rheumatoid arthritis: mechanisms, diagnosis and treatment. Nat Rev Rheumatol. 2012;8(11):656-64.
4. Hetland ML, Ejbjerg B, Hørslev-Petersen K, Jacobsen S, Vestergaard A, Jurik AG, et al. MRI bone oedema is the strongest predictor of subsequent radiographic progression in early rheumatoid arthritis. Results from a 2-year randomised controlled trial (CIMESTRA). Annals of the Rheumatic Diseases. 2009;68(3):384-90.
5. Carotti M, Galeazzi V, Catucci F, Zappia M, Arrigoni F, Barile A, et al. Clinical utility of eco-color-power Doppler ultrasonography and contrast enhanced magnetic resonance imaging for interpretation and quantification of joint synovitis: a review. Acta Biomed. 2018;89(1-S):48-77.
6. Burke CJ, Alizai H, Beltran LS, Regatte RR. MRI of synovitis and joint fluid. J Magn Reson Imaging. 2019;49(6):1512-27.
7. Ostergaard M, Boesen M. Imaging in rheumatoid arthritis: the role of magnetic resonance imaging and computed tomography. Radiol Med. 2019;124(11):1128-41.
8. Kirkhus E, Bjornerud A, Thoen J, Johnston V, Dale K, Smith HJ. Contrast-enhanced dynamic magnetic resonance imaging of finger joints in osteoarthritis and rheumatoid arthritis: an analysis based on pharmacokinetic modeling. Acta Radiol. 2006;47(8):845-51.
9. Wojciechowski W, Tabor Z, Urbanik A. Assessing synovitis based on dynamic gadolinium-enhanced MRI and EULAR-OMERACT scores of the wrist in patients with rheumatoid arthritis. Clin Exp Rheumatol. 2013;31(6):850-6.
10. Kobayashi Y, Kamishima T, Sugimori H, Ichikawa S, Noguchi A, Kono M, et al. Quantification of hand synovitis in rheumatoid arthritis: Arterial mask subtraction reinforced with mutual information can improve accuracy of pixel-by-pixel time-intensity curve shape analysis in dynamic MRI. J Magn Reson Imaging. 2018.
11. Sakashita T, Kamishima T, Kobayashi Y, Sugimori H, Tang M, Sutherland K, et al. Accurate quantitative assessment of synovitis in rheumatoid arthritis using pixel-by-pixel, time-intensity curve shape analysis. Br J Radiol. 2016;89(1061):20151000.
12. van de Sande MG, van der Leij C, Lavini C, Wijbrandts CA, Maas M, Tak PP. Characteristics of synovial inflammation in early arthritis analysed by pixel-by-pixel time-intensity curve shape analysis. Rheumatology (Oxford). 2012;51(7):1240-5.
13. Lavini C, de Jonge MC, van de Sande MG, Tak PP, Nederveen AJ, Maas M. Pixel-by-pixel analysis of DCE MRI curve patterns and an illustration of its application to the imaging of the musculoskeletal system. Magn Reson Imaging. 2007;25(5):604-12.
14. Kijowski R, Liu F, Caliva F, Pedoia V. Deep Learning for Lesion Detection, Progression, and Prediction of Musculoskeletal Disease. J Magn Reson Imaging. 2020;52(6):1607-19.
15. Wang H, Ou Y, Fang W, Ambalathankandy P, Goto N, Ota G, et al. A deep registration method for accurate quantification of joint space narrowing progression in rheumatoid arthritis. Computerized Medical Imaging and Graphics. 2023;108:102273.
16. Liang H, Lu Y, Liu Q, Fu X. Fully Automatic Classification of Cardiotocographic Signals with 1D-

CNN and Bi-directional GRU. Annu Int Conf IEEE Eng Med Biol Soc. 2022;2022:4590-4.
17. Hassan F, Hussain SF, Qaisar SM. Epileptic Seizure Detection Using a Hybrid 1D CNN-Machine Learning Approach from EEG Data. J Healthc Eng. 2022;2022:9579422.
18. Hsieh CH, Li YS, Hwang BJ, Hsiao CH. Detection of Atrial Fibrillation Using 1D Convolutional Neural Network. Sensors (Basel). 2020;20(7).
19. Aletaha D, Neogi T, Silman AJ, Funovits J, Felson DT, Bingham CO, 3rd, et al. 2010 Rheumatoid arthritis classification criteria: an American College of Rheumatology/European League Against Rheumatism collaborative initiative. Arthritis Rheum. 2010;62(9):2569-81.
20. Ostergaard M, Peterfy CG, Bird P, Gandjbakhch F, Glinatsi D, Eshed I, et al. The OMERACT Rheumatoid Arthritis Magnetic Resonance Imaging (MRI) Scoring System: Updated Recommendations by the OMERACT MRI in Arthritis Working Group. J Rheumatol. 2017;44(11):1706-12.
21. Ito K, Nakajima H, Kobayashi K, Aoki T, Higuchi T. A fingerprint matching algorithm using phase-only correlation. IEICE transactions on fundamentals of electronics, communications and computer sciences. 2004;87(3):682-91.
22. Reza AM. Realization of the contrast limited adaptive histogram equalization (CLAHE) for real-time image enhancement. Journal of VLSI signal processing systems for signal, image and video technology. 2004;38:35-44.
23. Bai S, Kolter JZ, Koltun V. An Empirical Evaluation of Generic Convolutional and Recurrent Networks for Sequence Modeling. ArXiv. 2018;abs/1803.01271.
24. van der Leij C, van de Sande MG, Lavini C, Tak PP, Maas M. Rheumatoid synovial inflammation: pixel-by-pixel dynamic contrast-enhanced MR imaging time-intensity curve shape analysis--a feasibility study. Radiology. 2009;253(1):234-40.
25. Ratner B. The correlation coefficient: Its values range between +1/−1, or do they? Journal of Targeting, Measurement and Analysis for Marketing. 2009;17(2):139-42.
26. Kubassova O, Boesen M, Cimmino MA, Bliddal H. A computer-aided detection system for rheumatoid arthritis MRI data interpretation and quantification of synovial activity. Eur J Radiol. 2010;74(3):e67-72.
27. Czaplicka K, Wojciechowski W, Wlodarczyk J, Urbanik A, Tabor Z. Automated assessment of synovitis in 0.2T magnetic resonance images of the wrist. Comput Biol Med. 2015;67:116-25.

Table

Classification Network
Input (1×27 one-dimensional time-intensity data)
Conv1D (128 8×1 filters, dilation rate=1), BN, SELU
Conv1D (256 5×1 filters, dilation rate=2), BN, SELU
Conv1D (128 3×1 filters, dilation rate=2), BN, SELU
GlobalAveragePooling (128)
Softmax (3 classes)

Table 1 Detailed network structure for the classification-based segmentation convolutional neural networks (CNNs) of the deep learning–based synovitis segmentation network. CNNs were built using the listed layers from the top to the bottom. Definitions of the different network structures and layers of the CNN have been described in a previously published article on deep learning applications in medical image analysis [23]. Conv1D = one-dimensional dilated causal convolution, BN = batch normalization, SELU = scaled exponential linear unit.

Figure Legends

Figure 1 Flowchart of time-intensity curve (TIC) extraction. The TIC data for muscle, bone, and synovitis were extracted using in-house developed software. The software takes DICOM data from dynamic contrast-enhanced magnetic resonance imaging (DCE-MRI) as input. By manually selecting layers and delineating regions of interest (ROIs) for muscle, bone, and synovitis, the software automatically generates TIC data for each pixel within the ROI and saves it as a CSV file.

Figure 2 Dynamic contrast-enhanced magnetic resonance imaging (DCE-MRI) preprocessing. The image undergoes a sequential three-stage pre-processing pipeline, which includes denoising, image enhancement, and image registration. Subsequently, the disease analysis involves extracting the time-intensity curve (TIC) for each pixel within the specified target region, utilizing the preprocessed image as a basis.

Figure 3 (A)1D convolutional neural network (CNN) architecture for the deep learning–based synovitis segmentation network. The network is designed to receive the time-intensity curve (TIC) curve of a pixel derived from dynamic contrast-enhanced magnetic resonance imaging (DEC-MRI) as input and generate the corresponding pixel classification result as output. The input TIC curve is reshaped into a 27-dimensional vector for efficient network input. The red lines serve as a set of examples demonstrating the workflow of the Dilated Causal Convolution kernel in our convolutional network. (B) The detail architecture of Dilated Causal Convolution Block in the segmentation network. SELU = scaled exponential linear unit.

Figure 4 Training and testing framework of the network, using a synovitis region as an example. For the training stage, the network undergoes comprehensive training using time-intensity curves (TICs) and corresponding labels of pixels. In the testing stage, the system receives a manually labeled bounding box as input. The network classifies individual pixels within the bounding box and synthesizes a segmentation mask, which is subsequently validated against the ground truth. Leave-one-out cross-validation is implemented by randomly shuffling the 28 patients (27 patients for training, 1 patient for testing). CNN = convolutional neural network, ZMN = zero-mean normalization.

Figure 5 Examples of the proposed segmentation network on the time-intensity curve characteristic curve. (A_1-B_4) Cases of Metacarpophalangeal (MCP) Joint, (C_{1-4}) One case of Distal Radioulnar Joint (DRUJ), (D_{1-4}) One case of Radiocarpal Joint (RCJ). Bounding box: Native dynamic contrast-enhanced magnetic resonance imaging (DCE-MRI) images of selected regions of interest, synovitis mask: ground truth from manual segmentation, Color Map: Enhancing pannus segmentation obtained from the network, Prediction: Overlapping regions of manual and automated segmentation. In prediction, red pixels represent manually segmented areas, blue pixels represent areas segmented automatically by the network, and green pixels represent regions where manual and automatic segmentation overlap.

Figure 6 Correlations between the synovitis volume outlined manually and the synovitis volume quantified by software at both pixel-based (Fig.6A: $r = 0.87$, $p < 0.001$) and patient-based levels (Fig.6B: $r = 0.84$, $p < 0.001$).

Figure 7 Bland-Altman analysis for the comparison of the volume of enhanced pannus for the manual outlining vs. network at both pixel-based (Fig.7A) and patient-based levels (Fig.7B).

Figure 8 Examples of the proposed segmentation network on the time-intensity curve characteristic curve in outlier cases. (A_{1-4}) One case of Distal Radioulnar Joint (DRUJ), (B_{1-4}) One case of Proximal Interphalangeal (PIP) Joint. Bounding Box: Native dynamic contrast-enhanced magnetic resonance imaging (DCE-MRI) images of selected region of interest, Synovitis mask: ground truth from manual segmentation, Color Map: Enhancing pannus segmentation obtained from the network, Prediction: Overlapping regions of manual and automated segmentation. In prediction, red pixels represent manually segmented areas, blue pixels represent areas segmented automatically by the network, and green pixels represent regions where manual and automatic segmentation overlap. In prediction, the white arrows indicate false negatives, the orange arrows indicate manual outlining errors made during the annotation process and the yellow arrows indicate false positives.

Figure 1

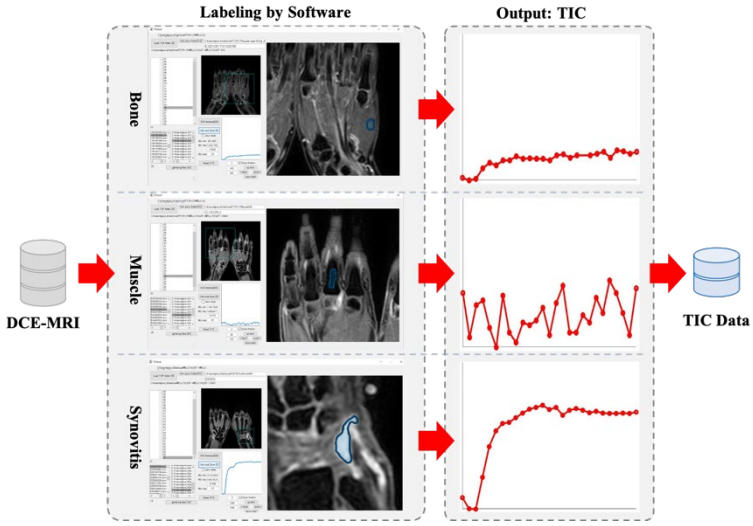
Labeling by Software
Output: TIC
Bone
Muscle
Synovitis
DCE-MRI
TIC Data

Figure 2

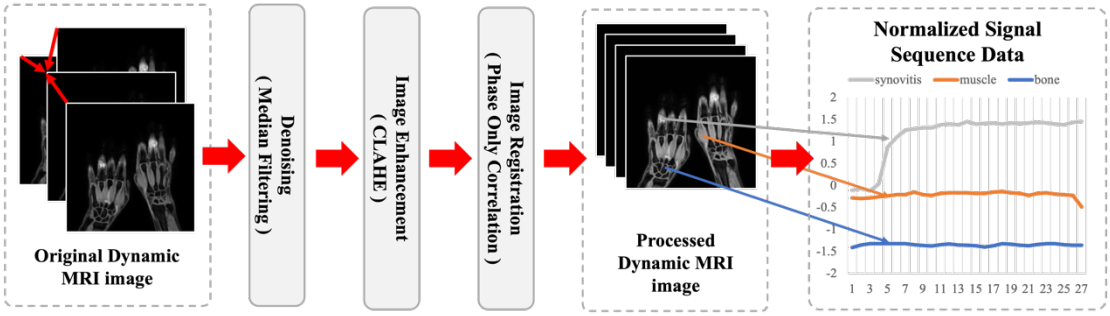
Original Dynamic MRI image
Denoising (Median Filtering)
Image Enhancement (CLAHE)
Image Registration (Phase Only Correlation)
Processed Dynamic MRI image
Normalized Signal Sequence Data
synovitis
muscle
bone
2
1.5
1
0.5
0
-0.5
-1
-1.5
-2
1 3 5 7 9 11 13 15 17 19 21 23 25 27

Figure 3

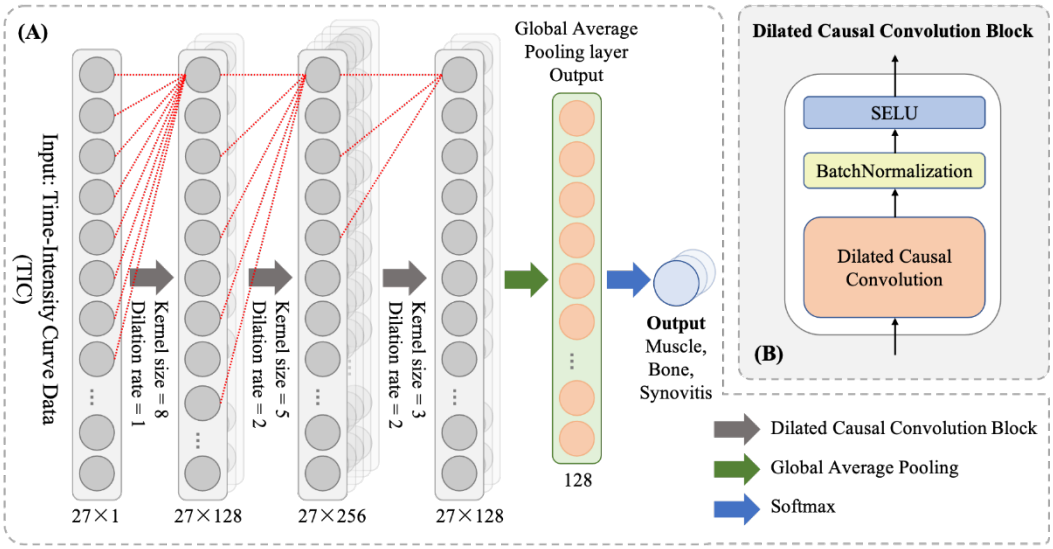
(A)
Input: Time-Intensity Curve Data (TIC)
Kernel size = 8
Dilation rate = 1
Kernel size = 5
Dilation rate = 2
Kernel size = 3
Dilation rate = 2
27×1
27×128
27×256
27×128
Global Average Pooling layer Output
128
Output
Muscle, Bone, Synovitis
Dilated Causal Convolution Block
SELU
BatchNormalization
Dilated Causal Convolution
(B)
Dilated Causal Convolution Block
Global Average Pooling
Softmax

Figure 4

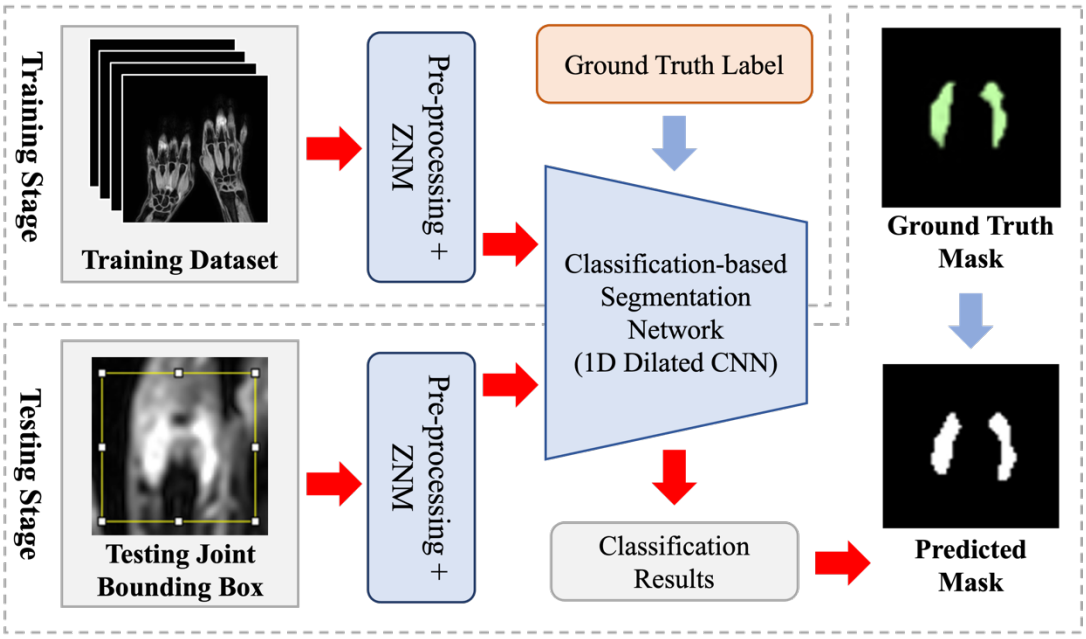
Training Stage
Training Dataset
Pre-processing + ZNM
Ground Truth Label
Classification-based Segmentation Network (1D Dilated CNN)
Ground Truth Mask
Testing Stage
Testing Joint Bounding Box
Pre-processing + ZNM
Classification Results
Predicted Mask

Figure 5

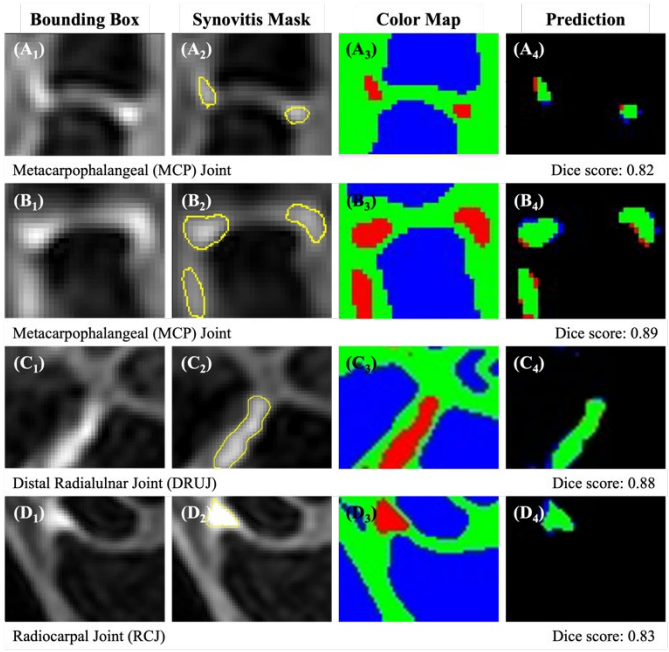
Bounding Box
Synovitis Mask
Color Map
Prediction
(A1)
(A2)
(A3)
(A4)
Metacarpophalangeal (MCP) Joint
Dice score: 0.82
(B1)
(B2)
(B3)
(B4)
Metacarpophalangeal (MCP) Joint
Dice score: 0.89
(C1)
(C2)
(C3)
(C4)
Distal Radialulnar Joint (DRUJ)
Dice score: 0.88
(D1)
(D2)
(D3)
(D4)
Radiocarpal Joint (RCJ)
Dice score: 0.83

Figure 6

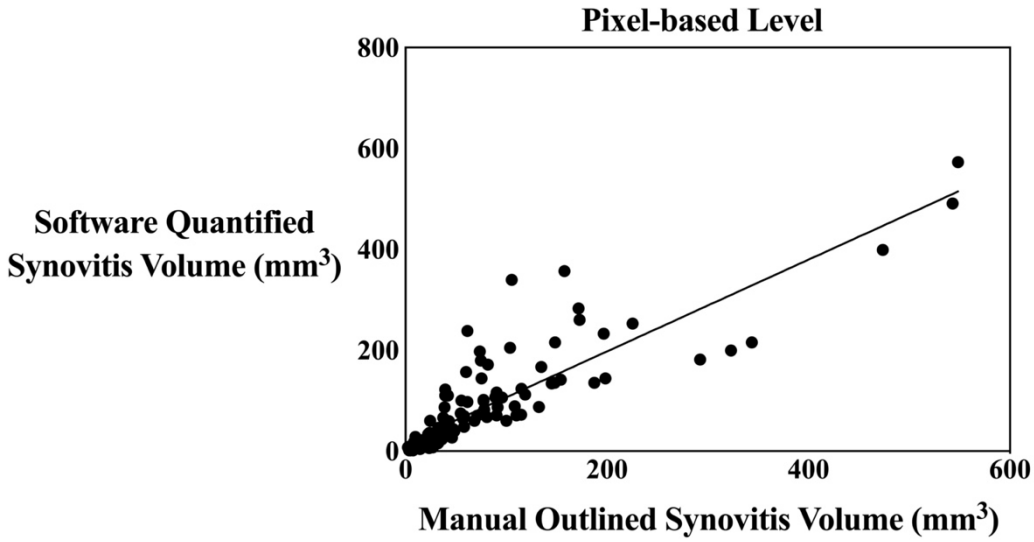
Pixel-based Level
Software Quantified Synovitis Volume (mm3)
800
600
400
200
0
0
200
400
600
Manual Outlined Synovitis Volume (mm3)

（A）

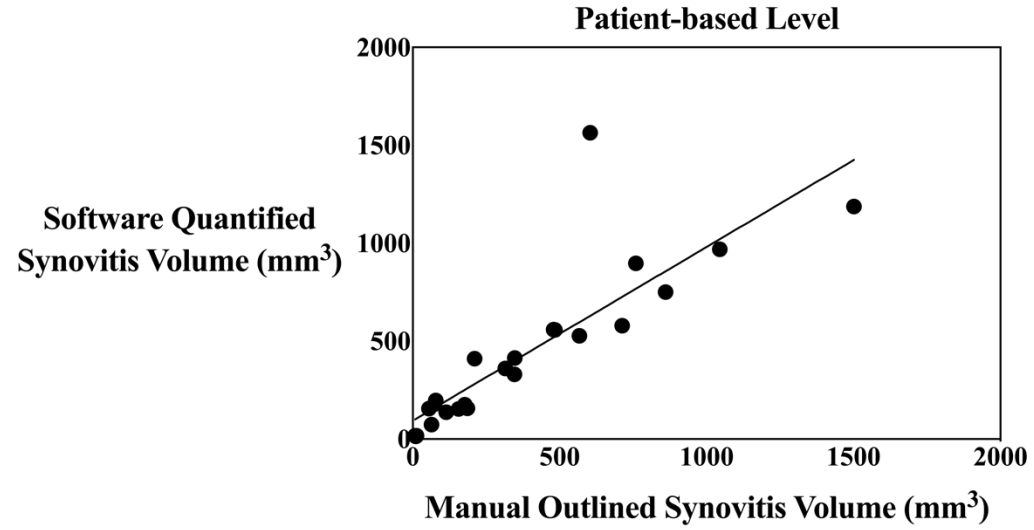
Patient-based Level
Software Quantified Synovitis Volume (mm3)
2000
1500
1000
500
0
0
500
1000
1500
2000
Manual Outlined Synovitis Volume (mm3)

(B)

Figure 7

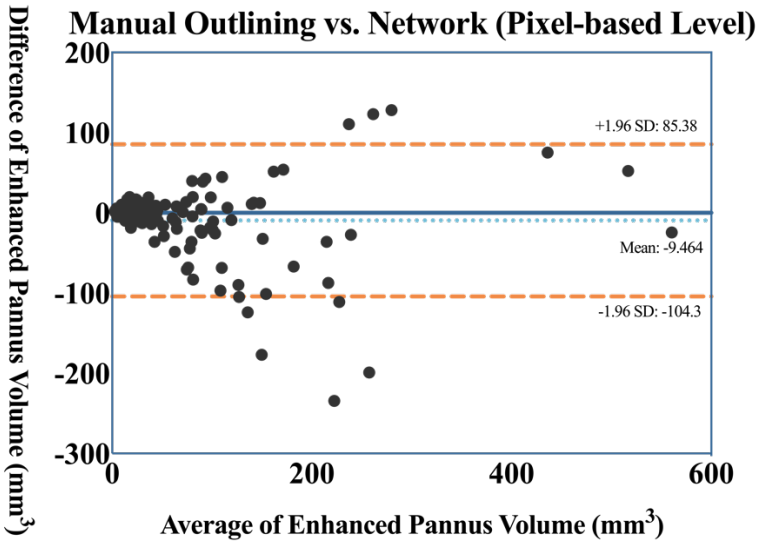
Manual Outlining vs. Network (Pixel-based Level)
Difference of Enhanced Pannus Volume (mm3)
200
100
0
-100
-200
-300
+1.96 SD: 85.38
Mean: -9.464
-1.96 SD: -104.3
0
200
400
600
Average of Enhanced Pannus Volume (mm3)

(A)

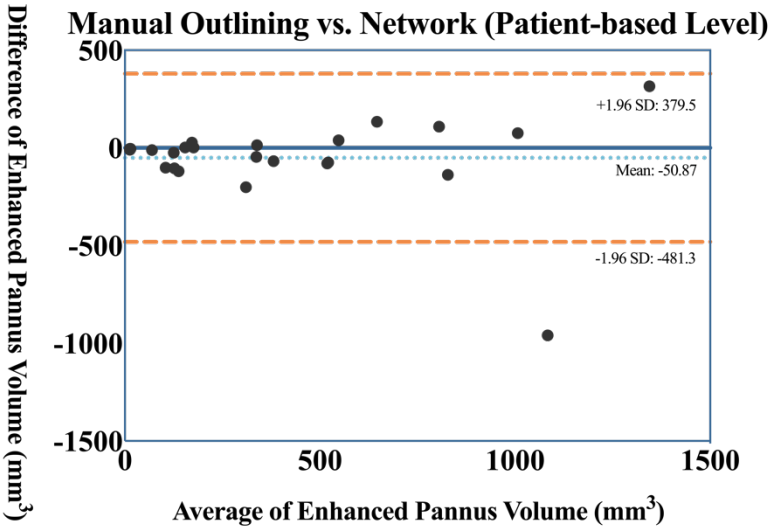
Manual Outlining vs. Network (Patient-based Level)
Difference of Enhanced Pannus Volume (mm3)
500
0
-500
-1000
-1500
+1.96 SD: 379.5
Mean: -50.87
-1.96 SD: -481.3
0
500
1000
1500
Average of Enhanced Pannus Volume (mm3)

(B)

Figure 8

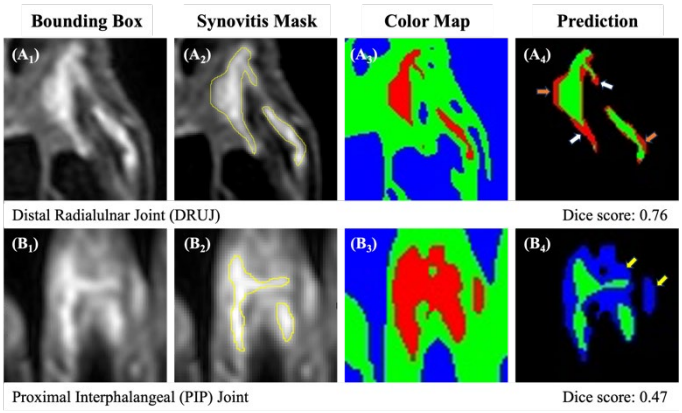
Bounding Box
Synovitis Mask
Color Map
Prediction
(A1)
(A2)
(A3)
(A4)
Distal Radialulnar Joint (DRUJ)
Dice score: 0.76
(B1)
(B2)
(B3)
(B4)
Proximal Interphalangeal (PIP) Joint
Dice score: 0.47